4678 J. Med. Chem. 2010, 53, 4678–4690
DOI: 10.1021/jm1002588

Journal of Medicinal Chemistry Article

Ruthenium−Porphyrin Conjugates with Cytotoxic and Phototoxic Antitumor Activity

Teresa Gianferrara,*[,†] Alberta Bergamo,*[,∥] Ioannis Bratsos,[‡] Barbara Milani,[‡] Cinzia Spagnul,[†] Gianni Sava,[∥,§] and Enzo Alessio[‡]

[†]*Department of Pharmaceutical Sciences, P.le Europa 1,* [‡]*Department of Chemical Sciences, Via L. Giorgieri 1, and* [§]*Department of Life Sciences, Via Giorgieri 7, University of Trieste, 34127 Trieste, Italy, and* [∥]*Callerio Foundation Onlus, Via A. Fleming 22-31, 34127 Trieste, Italy*

Received February 26, 2010

We report here two novel "extended-arms" porphyrins, TetbpyPP and TedabpyPP, in which four peripheral bpy fragments are connected to the *meso* positions of the macrocycle through flexible linkers of different length and hydrophilicity. We describe also the new, water-soluble, tetracationic conjugate [TedabpyPP{Ru([9]aneS3)Cl}$_4$][Cl]$_4$ (**6**). Compound **6** belongs to the series of cationic Ru−porphyrin conjugates **1**−**5**, each bearing four peripheral Ru(II) half-sandwich coordination compounds, that we recently prepared as potential photosensitizing chemotherapeutic agents. The in vitro cell growth inhibition of conjugates **1**−**6** toward MDA-MB-231 human breast cancer cells and HBL-100 human nontumorigenic epithelial cells are reported, together with the phototoxic effects of **1**, **4**, and **6** on MDA-MB-231 cells. All conjugates have IC_{50} values in the low micromolar range that decrease by 1 order of magnitude upon irradiation of cell cultures with visible light. The most promising compounds **1** and **6** are phototoxic at low light and drug doses.

Introduction

Ruthenium compounds have been investigated as potential anticancer agents in the last 35 years.[1] Two Ru(III) coordination compounds, NAMI-A and KP1019 (Figure 1),[2,3] both developed in the 1990s, have completed phase I clinical trials with promising results.[4,5] NAMI-A has started already a phase II combination study, whereas the sodium salt of KP1019, KP1339, was selected for further development because it is about 35 times more water soluble than its parent compound.

In general, these compounds showed a behavior quite different from that of cisplatin and the other established platinum anticancer chemotherapeutics, which makes them promising drug candidates with a distinct mode of action.[2,3] They were found to possess moderate or negligible cytotoxicity in vitro against cancer cells and exhibited peculiar activities in animal models: KP1019 showed excellent activity against platinum-resistant colorectal tumors,[3] whereas NAMI-A was found to be particularly active against the development and growth of metastases of solid tumors.[2,6]

In recent years, entirely new classes of organometallic Ru(II)−arene compounds, developed by the groups of Sadler,[7] Dyson,[8] Keppler,[9] and others,[10] were found to have promising anticancer activity both in vitro and, in some cases, also in vivo in murine models.[11] Interestingly, some of them proved to be active also against cisplatin-resistant xenografts.[7] Representative examples are [(η^6-biphenyl)Ru(en)Cl][PF_6] (RM175) and [(η^6-*p*-cymene)-$RuCl_2$(pta)] (RAPTA-C) (Figure 1). The geometry of these half-sandwich compounds can be described as pseudotetrahedral (*piano-stool* geometry). We demonstrated that replacement of the arene moiety of active half-sandwich organometallic compounds with a neutral face-capping 6-electron donor ligand, such as 1,4,7-trithiacyclononane, leads to coordination compounds that maintain a reasonable cytotoxicity in vitro.[12,13] For example, [Ru([9]aneS3)(en)Cl][CF_3SO_3] (Figure 1) was found to be ca. 10 times less cytotoxic than the corresponding organometallic compound RM175 against human breast cancer MDA-MB-231 cells. This result suggests that other neutral face-capping ligands might lead to increased activity. In other

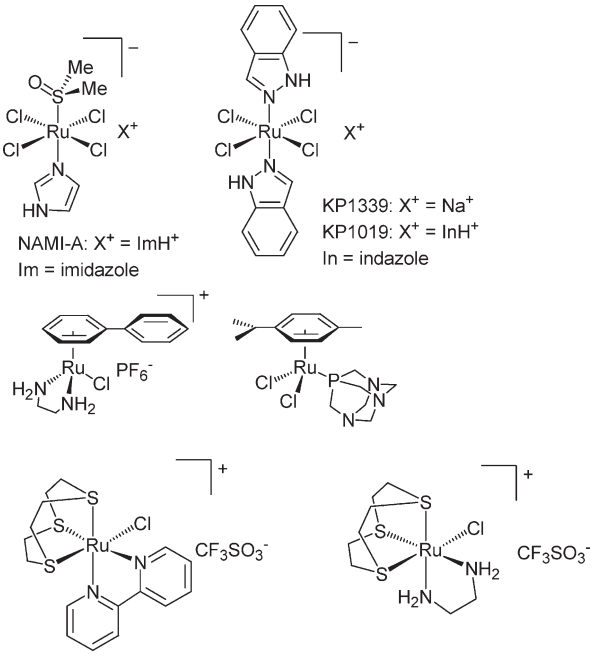

Figure 1. Schematic structures of NAMI-A (top, left), KP1019 and KP1339 (top, right), RM175 (middle, left), RAPTA-C (middle, right), [Ru([9]aneS3)(bpy)Cl][CF_3SO_3] (bottom, left), and [Ru([9]aneS3)(en)-Cl][CF_3SO_3] (bottom, right).

*To whom correspondence should be addressed. For T.G.: phone, +39 040.558.7859; fax, +39 040.525.72; E-mail, gianfer@units.it. For A. B.: E-mail, a.bergamo@callerio.org.

 Published on Web 05/21/2010

words, half-sandwich Ru(II) coordination compounds represent a new class of compounds that deserve a thorough investigation.

The conjugation of porphyrins to peripheral metal fragments is an intriguing strategy for making compounds that might combine the cytotoxicity of the metal moiety to the phototoxicity of the porphyrin chromophore for additive antitumor effects. Indeed, Brunner et al. synthesized hematoporphyrin− and tetraarylporphyrin−platinum derivatives and they found an increase of the antitumor activity of the platinum moiety by an additional light-induced toxicity.[14] More recently, Guo and co-workers described a dinuclear cisplatin−phthalocyanine conjugate that showed a remarkable enhancement of cytotoxicity against tumor cell lines when irradiated with red light.[15]

The central role of natural and synthetic porphyrins and metalloporphyrins in the photodynamic therapy of cancer (PDT[a]) is a well established issue.[16,17] PDT is a binary therapy for cancer treatment that involves the activation of a tumor-localized sensitizer with visible light.[18] In the absence of light, the photosensitizer should have negligible effect on either healthy or tumor cells. However, when the drug-localized tissue is irradiated, the drug becomes activated and the tissue is rapidly destroyed. Thus, this technique offers precise spatial and temporal control over drug activation and can, in principle, selectively target and destroy abnormal tissue in the presence of normal tissue, provided that the light beam is carefully applied. In the presence of endogenous oxygen, energy transfer from an excited state of the photosensitizer can lead to a series of photochemical reactions and generation of various cytotoxic species (e.g., singlet oxygen and other reactive oxygen species, ROS) and consequently induce apoptosis and necrosis of targeted cells and tissues (type-II PDT).[19−21] There is also a rapidly growing interest in the new field of inorganic photoactivated chemotherapy (PACT), i.e., in the development of complexes of different *d*-block metals, and in particular ruthenium, that acquire anticancer activity upon photoexcitation.[22]

Some water-soluble porphyrins and metallo-porphyrins show also conventional anticancer activity.[23] The most relevant example is the Au(III) porphyrin [Au^{III}(TPP)]Cl, extensively investigated by Che and co-workers,[24] that shows potent in vitro anticancer properties toward a range of human cancer cell lines, with some selectivity for cancer cells over normal cells, and exhibits promising in vivo activity against hepatocellular carcinoma and nasopharyngeal carcinoma. The cytotoxicity is not enhanced by light irradiation (i.e., no PDT activity) and depends critically on the presence of Au(III) because [Zn^{II}(TPP)] is at least 100-fold less active than [Au^{III}(TPP)]Cl under the same conditions.

In addition to conventional and PDT activity, metal−porphyrin conjugates might have some other positive features such as tumor selectivity. In fact, porphyrins typically show preferential uptake and retention by tumor tissues, possibly via receptor-mediated endocytosis of low density lipoproteins (LDL).[25] Thus, porphyrins might behave as carrier ligands for the active transport of anticancer metal compounds into cancer cells. In addition to the tumor-localizing properties of porphyrins, in vivo these relatively large Ru−porphyrin conjugates might exploit the unique extracellular environment of tumors (e.g., their defective vasculature) and benefit of the so-called "enhanced permeability and retention" (EPR) effect for an increased passive targeting of malignant tissues.[26] Photoexcitation of the organic chromophore, followed by energy and/or electron transfer to the peripheral metal centers, might also induce their activation, e.g. through dissociation of ligands, and consequently lead to a reactivity different than in the dark.[27] Furthermore, provided that the conjugates are sufficiently stable, the fluorescence emission of the chromophore might be exploited for tracking the biodistribution of the metal in the extra- and intracellular environment of malignant cells through fluorescence microscopy. Finally, an appropriate choice of the peripheral metal fragments might considerably improve the water solubility of the porphyrins, an important feature for biomedical applications.

For the reasons detailed above, it is of great interest to study the anticancer properties of porphyrin−ruthenium conjugates. Therrien and co-workers recently reported that neutral conjugates of *meso*-pyridylporphyrins with organometallic [Ru(η^6-arene)Cl_2] fragments are moderately cytotoxic in the dark against Me300 human melanoma cells and become cytotoxic upon irradiation with visible light.[28] Similar results were reported also by Swavey and co-workers for cationic conjugates bearing from 1 to 4 [Ru(bpy)$_2$Cl]$^+$ fragments.[29]

More recently, we described the preparation and characterization of several new Ru−porphyrin conjugates that bear either negatively charged NAMI-A-type Ru(III) fragments or positively charged half-sandwich Ru(II) coordination compounds.[30] The connection between the tetrapyrrolic macrocycle and each peripheral metal center occurred either through a single N(pyridyl)−Ru bond or through a chelating bpy unit (Figure 2). Both approaches have positive and negative aspects: the single-bond connection allowed us to use the commercially available *meso*-4′-tetrapyridylporphyrin (4′TPyP), whereas the preparation of the *meso*-(*p*-bpy-phenyl)porphyrins (bpy$_n$-PPs, n = 1−4, Figure 2) required multistep synthetic procedures. On the other hand, conjugation through a single bond, while leaving five, rather than four, coordination positions on Ru available for functionalization, is intrinsically less stable than chelation through bpy and might lead to loss of the peripheral Ru fragments under in vivo conditions.

Out of the above-mentioned porphyrin−Ru conjugates, we selected the five cationic compounds described in Figure 3, representative of both types of connections, for biological tests. Compounds **1**, **2**, and **5** bear coordinatively saturated Ru compounds, whereas **3** and **4** have half-sandwich Ru fragments with a relatively labile DMSO ligand and are therefore, in principle, more prone to coordination to biological targets. All conjugates are either soluble in water (**1**) or in DMSO (**2**−**5**); those conjugates that are not well soluble in aqueous solution usually become moderately soluble in phosphate buffer at physiological

[a] Abbreviations: AAS, atomic absorption spectroscopy; bpy, 2,2′-bipyridine; Boc, *tert*-butoxycarbonyl; bpyAc, 4-methyl-2,2′-bipyridine-4′-carboxylic acid; bpy$_n$-PP, *meso*-(*p*-bpy-phenyl)porphyrin; DAPI, 4′,6-diamidino-2-phenylindolyl hydrochloride; DMA, 9,10-dimethylanthracene; DMAP, dimethylaminopyridine; DMF, *N*,*N*-dimethylformamide; DMSO, dimethyl sulfoxide; DSS, 2,2-dimethyl-2,2-silapentane-5-sulfonate; EDCI, *N*-(3-dimethylaminopropyl)-*N*′-ethylcarbodiimide hydrochloride; EDTA, ethylenediaminetetraacetic acid; en, ethane-1,2-diamine; EPR, enhanced permeability and retention; FBS, fetal bovine serum; HOBt, 1-hydroxybenzotriazole; Hp, hematoporphyrin; LDL, low-density lipoprotein; MTT, thiazolyl blue tetrazolium bromide; PACT, photoactivated chemotherapy; PBS, phosphate-buffered saline; PDT, photodynamic therapy; pta, 1,3,5-triaza-7-phosphatricyclo[3.3.1.1]decane; ROS, reactive oxygen species; 4′TCMePP, *meso*-4′-tetracarboxymethylphenylporphyrin; TCPP, *meso*-4′-tetracarboxyphenylporphyrin; TFA, trifluoroacetic acid; THF, tetrahydrofuran; TPP, *meso*-tetraphenylporphyrin; 4′TPyP, *meso*-4′-tetrapyridylporphyrin.

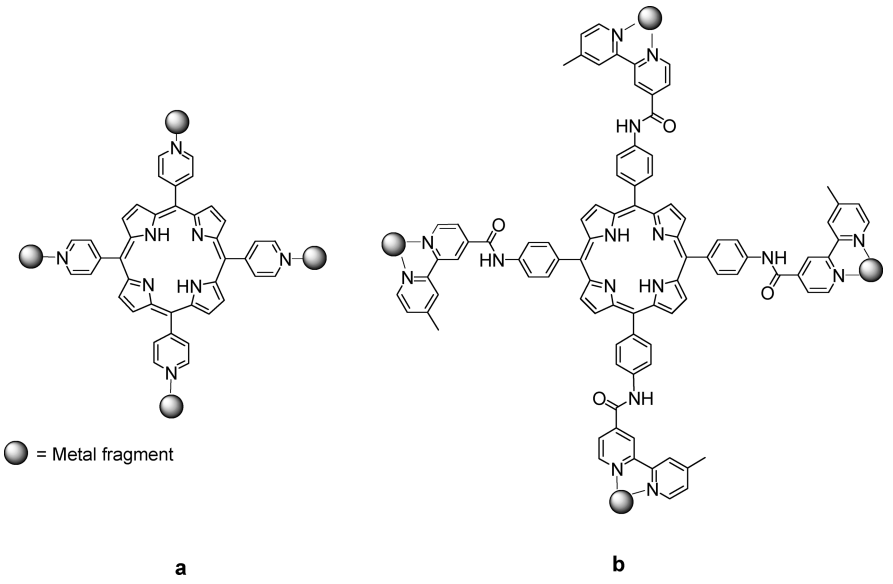

Figure 2. Metal−porphyrins conjugates through single bond (a) or multiple bonds (b).

pH or upon addition of small amounts of DMSO. We also found that the peripheral Ru moieties do not quench the porphyrin fluorescence emission significantly.[30]

With the aim of expanding the number and chemical features of the tetrapyrrolic chromophores suitable for conjugation with Ru fragments, we describe here two novel "extended-arms" versatile porphyrins, namely TetbpyPP and TedabpyPP (Scheme 1), in which the four peripheral bpy fragments are connected to the *meso* positions of the macrocycle through flexible linkers of different length and hydrophilicity.

In addition, we report also the synthesis and characterization of the new, water-soluble, tetracationic Ru-TedabpyPP conjugate [TedabpyPP{Ru([9]aneS3)Cl}$_4$][Cl]$_4$ (**6**), together with the in vitro cell growth inhibition of compounds **1**−**6** in human breast cancer MDA-MB-231 and in human nontumorigenic HBL-100 cells, and the phototoxic effects of **1**, **4**, and **6** on MDA-MB-231 cells upon irradiation with visible light (590−700 nm).

Results and Discussion

Synthesis and Characterization. Basically, the same multistep synthetic route was followed to obtain the two new extended-arm porphyrins, TetbpyPP and TedabpyPP (Scheme 1), that bear four peripheral bpy fragments connected at the *meso* positions through flexible linkers. First, the condensation of pyrrole and methyl 4-formyl benzoate,[31] followed by hydrolysis in basic conditions in THF/CH_3OH, gave the *meso*-4′-tetracarboxyphenylporphyrin (TCPP). The hydroxybenzotriazole (HOBt) ester of TCPP was then coupled with either *N*-Boc-2,2′-diethylamine (yield 60%) or *N*-Boc-2,2′-(ethylenedioxy)-diethylamine (yield 72%) in DMF. These intermediates (TetNHBocPP and TedaNHBocPP, respectively) were quantitatively deprotected using TFA in CH_2Cl_2 and then coupled with 4-methyl-2,2′-bipyridine-4′-carboxylic acid (bpyAc) in the same experimental conditions, giving TetbpyPP (74%) or TedabpyPP (96%), respectively. The extended-arm bpy-porphyrins were characterized by UV−vis and ^{1}H NMR spectroscopy and by electrospray mass spectrometry (see Figures S1−S4 in the Supporting Information). Both porphyrins are well soluble in DMSO but insoluble in water (even upon addition of small amounts of DMSO), so that comparative biological tests could not be performed.

Treatment of either porphyrin with 4 equiv of the neutral Ru(II) precursor [Ru([9]aneS3)(dmso)Cl$_2$] in refluxing CH_2Cl_2/CH_3OH mixtures afforded, upon replacement of the dmso and of a chloride ligand by bpy, the corresponding tetraruthenated compound in excellent yield: [TedabpyPP{Ru([9]aneS3)Cl}$_4$]-Cl$_4$ (**6**) (Figure 4) or [TetbpyPP{Ru([9]aneS3)Cl}$_4$]Cl$_4$ (**7**) (Figure S3 in Supporting Information), respectively. Both the tetracationic ruthenium conjugates **6** and **7** were characterized by mono- (Figure S4 in Supporting Information) and bidimensional ^{1}H NMR spectroscopy (Figure 5).

Even though compound **6** has a good solubility in water, its proton NMR spectrum in D_2O presents only broad peaks, possibly due to aggregation occurring at NMR concentrations as previously observed with other Ru−porphyrin conjugates.[32] For this reason, the NMR spectra of both compounds were recorded in DMSO-d_6, where only sharp resonances are observed. In general, the NMR spectra of both conjugates are consistent with their expected 4-fold symmetry, i.e., all peripheral Ru fragments are equivalent.[30] The ^{1}H NMR spectrum of **6** in the upfield region shows, beside the multiplets of [9]aneS3 (δ = 2.40−2.85), a singlet at δ = 2.53 for the methyl on bpyAc and the multiplets of the aliphatic spacer (δ = 3.55−3.70). The two internal NH pyrrole protons appear as a relatively broad singlet at $\delta \approx -2.9$. In the downfield region, the six resonances of the bpyAc protons maintain the same relative pattern as in the free TedabpyPP (even though, as typical for these compounds, they are slightly broader than those in the free porphyrin). While the resonances of H5,5′ are scarcely affected by coordination to Ru, those of H6,6′ and H3,3′ are shifted downfield by ca. 0.5 ppm. Also, the two triplets of the amide NH protons are remarkably shifted downfield (ca. 2 ppm compared to free TedabpyPP), but this effect is most likely due to the change of solvent (DMSO-d_6 vs CD_2Cl_2). The correlation H−H COSY spectrum of **6** (Figure 5) displays two strong cross peaks between vicinal bipyridyl protons (H5 and H6, H5′ and H6′), and two weaker peaks between the multiplets for the CH_2 protons of the spacer and the NH amide protons. The ^{1}H NMR spectrum of **7** displays several overlapping resonances for the bpyAc protons, and only those of H5,5′ are well

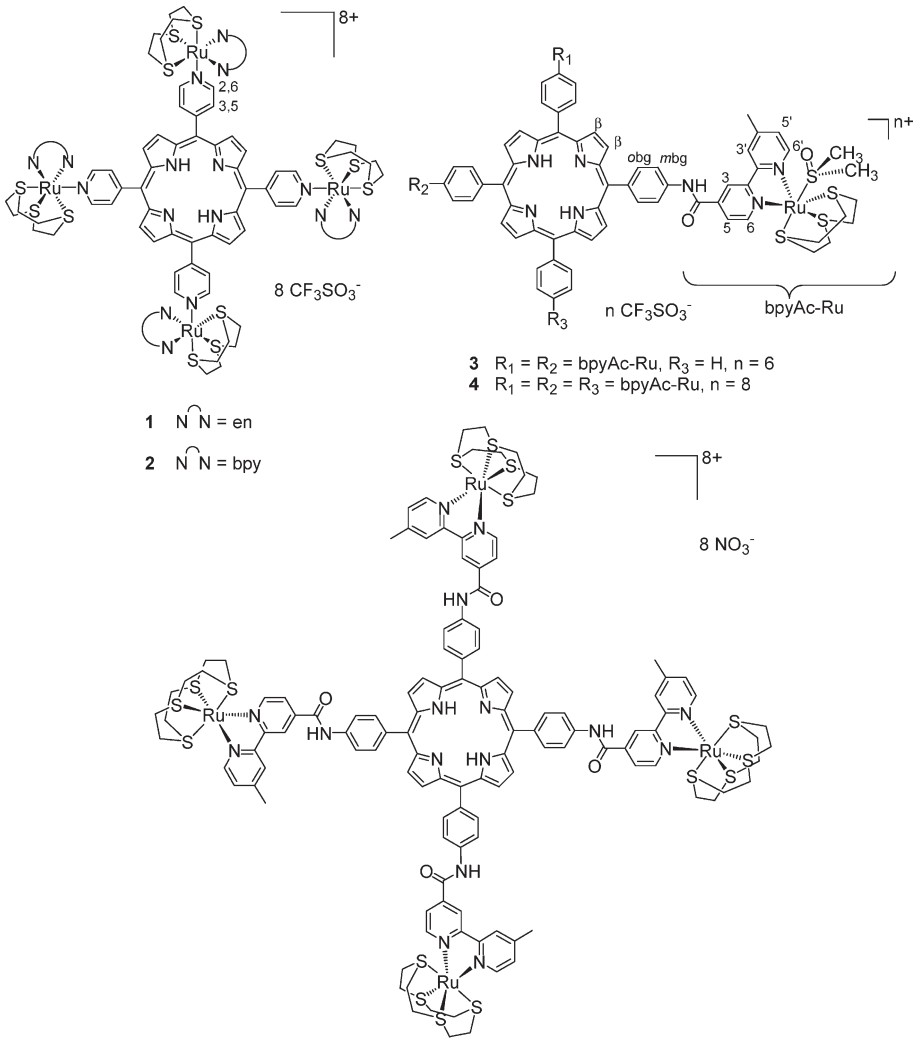

Figure 3. Schematic structures of ruthenium−porphyrin conjugates **1**−**5**.

resolved (Figure S4 in Supporting Information). Owing to its low solubility in water, compound **7** was not investigated further.

Consistent with what was observed already for compound **4**, the fluorescence spectrum of **6** is very similar to that of the parent porphyrin TedabpyPP, except for the ca. 25% quenching of the emission intensity attributed to the peripheral heavy atoms (Figure S5 in Supporting Information). The fluorescence properties of porphyrins are useful to study their aggregation behavior in solution. In fact, porphyrins in their monomeric form usually show intense fluorescence emissions, which are partially or completely quenched upon aggregation in solution.[33] The fluorescence spectra of optically matched (0.2 A) solutions of **6** in either DMSO or water showed an emission band at 648 nm upon excitation of the Soret band; the significant reduction in emission intensity on going from DMSO to H_2O ($\approx$ 60%) suggests that the ruthenium−porphyrin conjugate partially aggregates in water (Figure S5 in Supporting Information). This finding is consistent with the very low resolution of the ^1H NMR spectrum in D_2O.

The time course of the UV−vis spectrum of **6** in aqueous solution was recorded at 25 °C. The Soret band absorbance gradually increased ($\approx$ 14%) until an almost constant value was reached after 3 h (Figure S6 in Supporting Information). No shape modification or shift of the Soret band were observed, suggesting that no major chemical modification of the porphyrin structure is occurring and that the minor absorbance increase might be due to chloride hydrolysis and formation of the Ru−aquo species (Figure S6 in Supporting Information).[12]

Cell Culture Studies. The cytotoxicity of compounds **1**−**6**, in the dark, was evaluated in the human breast cancer cells MDA-MB-231 and in the nontumorigenic epithelial cells HBL-100 after an exposure of 72 h. The IC_{50} values are reported in Table 1 and are compared with those obtained by treating cells with two half-sandwich Ru(II) complexes that closely mimic the peripheral fragments on the conjugates: [Ru([9]aneS3)-(en)Cl][CF_3SO_3] (**8**) and [Ru([9]aneS3)(bpy)Cl][CF_3SO_3] (**9**) (Figure 1). While the reference Ru complexes are either mildly (**8**) or not cytotoxic at all (**9**), the Ru−porphyrin conjugates **1**−**5** show IC_{50} values in the low micromolar range (2−10 μM), i.e., up to 2 orders of magnitude lower than those measured for **8**. Compound **6** is slightly less active in reducing cell proliferation as it shows, in both cell lines, IC_{50} values statistically higher than those of the other conjugates. Taken together, these results show that, even when the cell growth inhibition per Ru

Scheme 1. Synthetic Route to TetbpyPP and TedabpyPP[a]

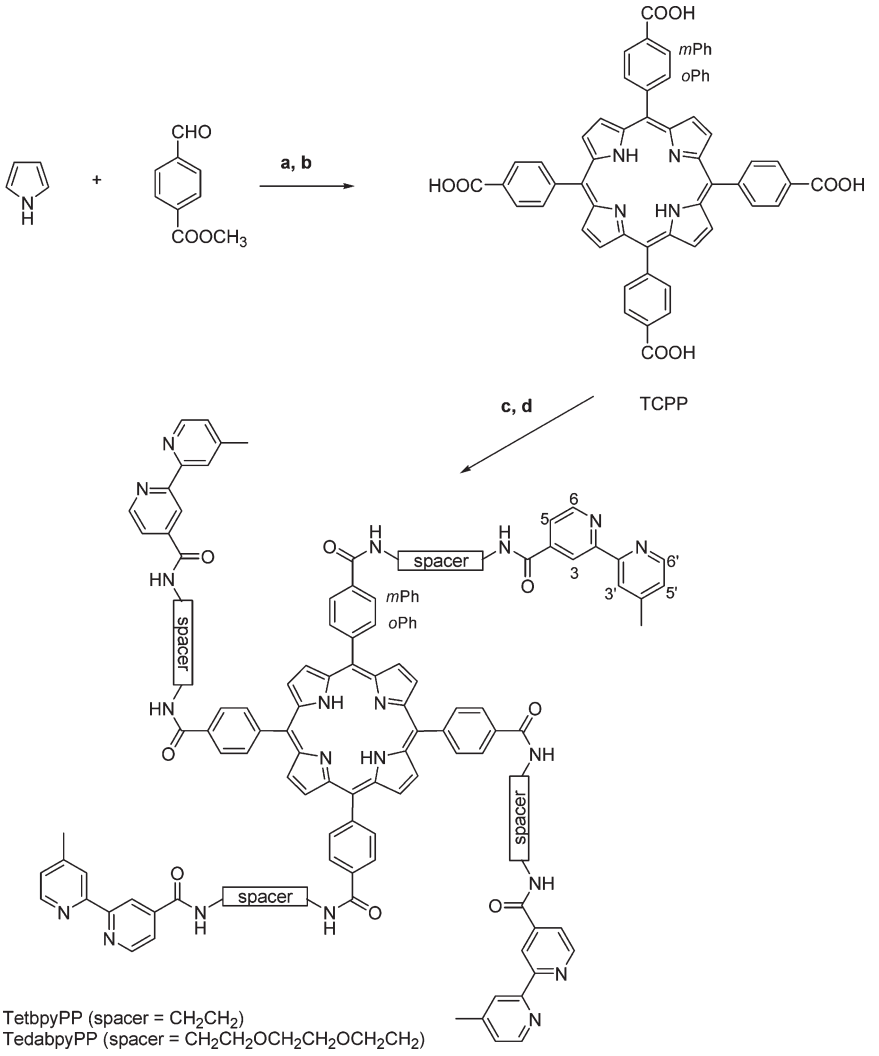

[a] Reactions and conditions: (a) propionic acid, reflux, 1.5 h (21%); (b) KOH aq 40%, THF/CH_3OH 2:1, 40 °C, 1 h (93%); (c) EDCI/HOBt/DMAP, $NH_2CH_2CH_2OCH_2CH_2OCH_2CH_2NHBoc$ (72%) DMF, rt, 24 h or EDCI/HOBt, $NH_2CH_2CH_2NHBoc$, DMF, rt, 2.5 h, then TFA, rt, 2 h (100%); (d) EDCI/HOBt/DMAP, bpyAc, DMF, rt, 24 h (96% and 74%).

fragment is considered, conjugates **1**−**6** remain remarkably more cytotoxic compared to the reference Ru complexes. In addition, their cytotoxic activity seems to be scarcely dependent on the type of porphyrin−Ru connection, on the number of ruthenium fragments on the periphery of the porphyrin (compare **3** vs **4**), on the total positive charge of the adduct, and on the hydrophilicity (**1** and **6** have good water solubility). These observations suggest that the increase of cytotoxic potency of the porphyrin conjugates with respect to the Ru complexes might derive from an improved uptake in cancer cells.[34] In addition, the cell growth inhibition, which is apparently also independent of the presence of substitutionally labile ligands on the ruthenium fragments (compare **1**, **2** and **5** vs **3**, **4** and **6**), probably does not involve direct coordination of the conjugates to biological targets. The finding of cytotoxic activity in substitutionally inert metal complexes, which apparently contradicts the paradigms established for anticancer Pt compounds, is becoming an increasingly common feature in modern inorganic anticancer research.[35] Also in the case of $[Au^{III}(TPP)]Cl$ it has been proposed that the compound, which is stable under physiological conditions, interacts with biomolecular targets through noncovalent interactions behaving essentially as an organic lipophilic cation.[24]

Whereas for **1**−**3** and **5** the IC_{50} values are substantially independent of the cell line being treated, compounds **4** and **6** are ca. two times more active against the highly invasive tumor MDA-MB-231 cells than against the nontumorigenic HBL-100 cells, with IC_{50} values of approximately 5 and 10 μM for compound **4** (p = 0.0283 for MDA-MB-231 vs HBL-100), and of 12 and 26 μM for compound **6** (p = 0.0009 for MDA-MB-231 vs HBL-100), respectively. Despite what might be a first-sight impression, the half-sandwich Ru fragments of compounds **4** and **6** are remarkably similar: the investigation performed on the reference complexes [Ru([9]aneS3)(bpy)Cl][CF_3SO_3] (**9**) and [Ru([9]-aneS3)(bpyAc)(dmso)][$CF_3SO_3]_2$ (**10**) showed that both DMSO and Cl are relatively labile ligands that are released in aqueous solution.[12,30] Consistently, both **4** and **6**, under in vivo conditions, are likely to generate the same peripheral [Ru([9]aneS3)-(bpyAc-P)(H_2O)]$^{2+}$ (P = porphyrin) fragments (see above for **6**). Thus, the main structural difference of **6** compared to **4** are the flexible hydrophilic spacers between the chromophore and the peripheral Ru fragments. Apparently, this feature makes **6** less cytotoxic but preserves its capability to distinguish

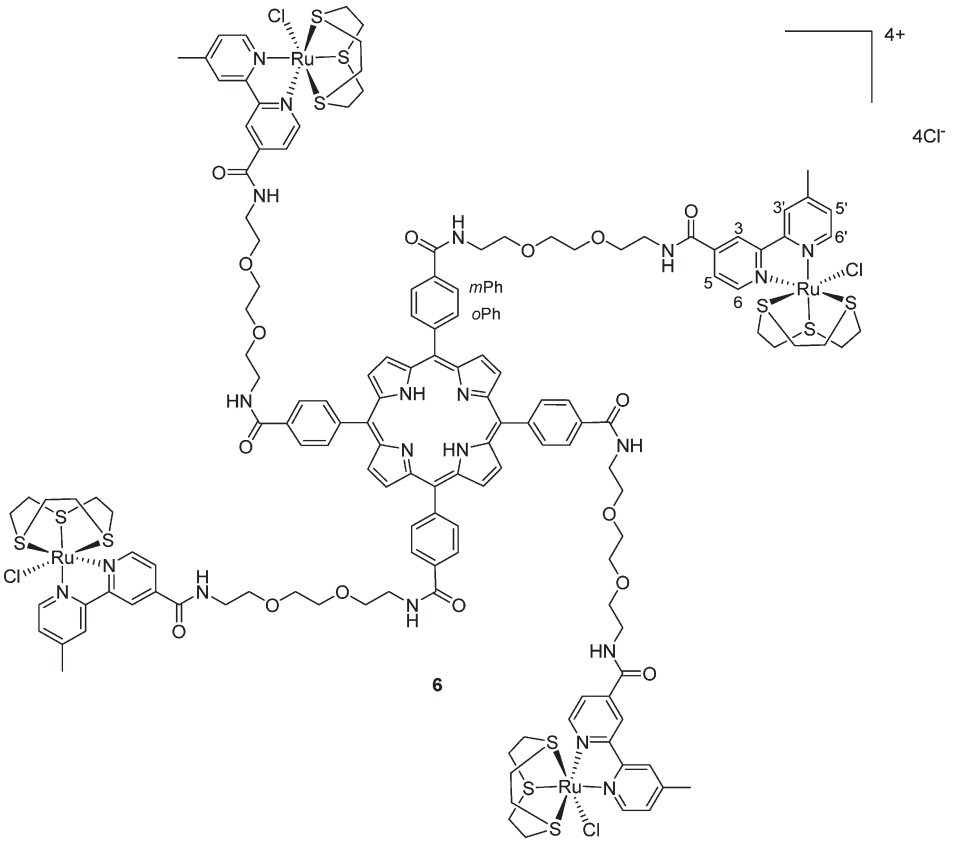

Figure 4. Schematic structure of the ruthenium−porphyrin conjugate **6**.

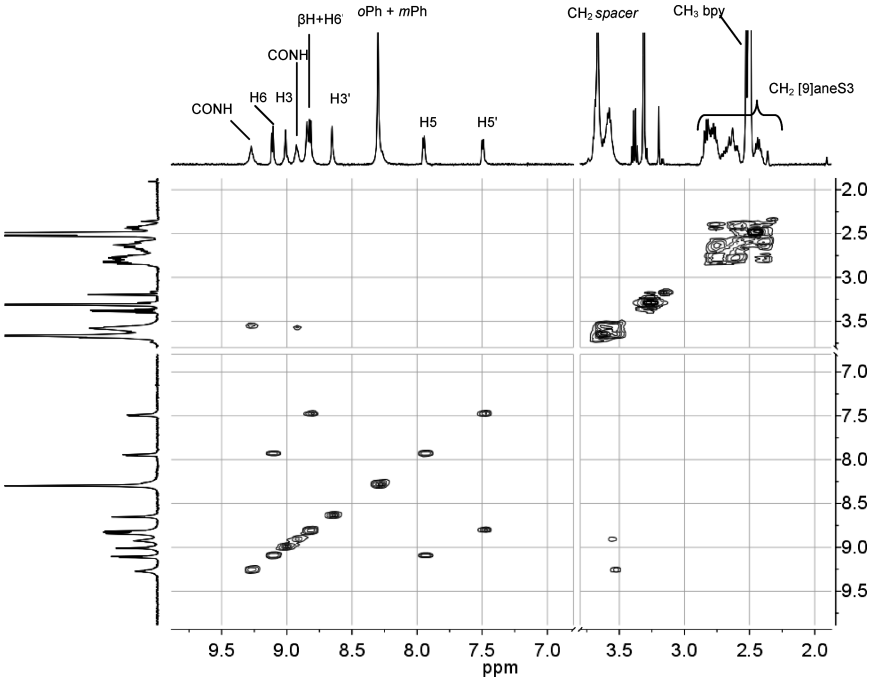

Figure 5. H−H COSY NMR spectrum of **6** in DMSO-d_6. See Figure 4 for numbering scheme.

between the nontumorigenic HBL-100 and the highly invasive MDA-MB-231 cell line showing selectivity against this latter. This finding suggests that compounds **4** and **6** might have a specific interaction with a target differently expressed by the two cell lines.

Phototoxicity. Conjugates **1**, **4**, and **6** were selected for performing a detailed investigation of their cytotoxic activity against MDA-MB-231 human breast cancer cells under irradiation with visible light (phototoxicity). These compounds, beside being soluble in DMSO, are also well (**1** and **6**), or at least appreciably (**4**), soluble in water, and represent three types of porphyrins with increasing structural complexity and both types of porphyrin−Ru connections. The cell cultures were exposed for 24 h at concentrations of the

Table 1. IC_{50} Values of Tested Compounds on MDA-MB-231 and HBL-100 Cells after 72 h Treatment (in the Dark)[a]

	IC_{50} [μM]	
	MDA-MB-231	HBL-100
1	4 ± 1	2 ± 1
2	5−5	4−5
3	4−5	6−8
4	4−6	10−10
5	4−5	6−7
6	12 ± 2	26 ± 2
[Ru([9]aneS3)(en)Cl][CF_3SO_3] (**8**)	146−177[b]	175[c]
[Ru([9]aneS3)(bpy)Cl][CF_3SO_3] (**9**)	> 300[b]	nd

[a] MDA-MB-231 cells grown in multi-well plates were treated with compounds **1**−**6** at 0.1 μM ÷ 30 μM for 72 h, then cell cytotoxicity was detected by MTT. IC_{50} are the mean ± SD calculated from values obtained in three separated experiments (compounds **1**, **6**) or the values obtained in two separate experiments (compounds **2**, **3**, **4**, **5**). Statistics: unpaired t test. [b] From ref 13. [c] From ref 12.

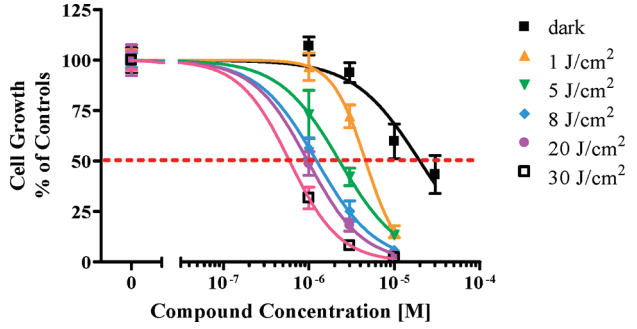

Figure 6. Light dose−effect curves for **6** as representative ruthenium−porphyrin conjugate. MDA-MB-231 human breast cancer cells were exposed to doses from 1 to 10 μM for 24 h, then cells were irradiated at a fluence rate of 25 mW/cm^2 and total light doses ranging from 1 to 30 J/cm^2. Cell cytotoxicity was determined 24 h after the end of irradiation by MTT test. The dotted line corresponds to 50% inhibition of cell proliferation.

conjugates ranging from 0.1 to 10 μM, then were irradiated at 590−700 nm with a fluence rate of 25 mW/cm^2 and light doses from 1 to 10 J/cm^2. The exposure of control cells to these total light doses does not induce an inhibition of cell proliferation as reported in Figure S7 (see Supporting Information). Cell cytotoxicity was determined using the MTT test 24 h after the end of the irradiation. Cells treated with the same concentrations of the test compounds, but kept in the dark, were used as controls for photocytotoxicity, whereas cells neither exposed to drugs nor to light were used as controls for cytotoxicity. The optimal total light dose was determined in a preliminary series of experiments using **6** as representative ruthenium−porphyrin conjugate (Figure 6). By irradiating the tumor cells at increasing total light doses from 1 to 30 J/cm^2, the dose−response curve shifts to the left and the IC_{50} value correspondingly decreases. Light doses greater than 10 J/cm^2 were discarded because of induced excessive toxicity.

The phototoxicity of compounds **1**, **4**, and **6** against MDA-MB-231 cells at increasing total light doses is shown in Table 2. IC_{50} values are compared to those calculated from cell cultures similarly treated with the Ru−porphyrin conjugates but kept in the dark. For example, compound **1** has an IC_{50} of 3.34 μM in the dark, that becomes 1.73 μM, 0.29 μM ($p < 0.05$ vs dark), and 0.13 μM ($p < 0.05$ vs dark) when cells are exposed to 1 J/cm^2, 5 J/cm^2, and 10 J/cm^2, respectively. Similar results were observed for compound **6**, whose IC_{50} drops from 2.09 μM (dark) to 0.10 μM (10 J/cm^2, $p < 0.01$ vs dark). Under these

Table 2. IC_{50} Values of Compounds **1**, **4**, and **6** in MDA-MB-231 Cells Treated for 24 h and Then Exposed to Increasing Doses of Visible Light (590−700 nm)[a]

	IC_{50} [μM]			
	dark	1 J/cm^2	5 J/cm^2	10 J/cm^2
1	3.34 ± 1.87	1.73 ± 1.10	0.29 ± 0.02	0.13 ± 0.04
4	24.62 ± 6.38	10.64 ± 1.61	3.93 ± 1.24	1.71 ± 0.64
6	2.09 ± 0.78	0.56 ± 0.12	0.24 ± 0.10	0.10 ± 0.04

[a] MDA-MB-231 cells grown in multi-well plates were treated with compounds **1**, **4**, and **6** at 0.1−10 μM for 24 h, then cells were irradiated with visible light (590−700 nm) at 25 mW/cm^2 fluence rate and total light doses of either 1 J/cm^2, 5 J/cm^2 or 10 J/cm^2. Cell cytotoxicity was detected by MTT test 24 h after irradiation. Statistics: ANOVA Analysis of variance and Tukey−Kramer post test.

experimental conditions, compound **4** is slightly less active than the others when cells are kept in the dark (IC_{50} = 24.62 μM) but, after light exposure, its IC_{50} value decreases by 1 order of magnitude, similarly to the other two compounds: 1.71 μM at 10 J/cm^2 ($p < 0.001$ vs dark, and $p < 0.05$ vs 1 J/cm^2).

It should be noted that the experimental conditions used in these experiments for determining the cytotoxicity in the dark (i.e., 24 h of cell challenge with each compound followed by further 24 h in a drug free medium and evaluation by the MTT test) are different from those described above (i.e., 72 h continuous drug treatment followed by the MTT test). The two schedules do not affect the IC_{50} of **1** but yield moderately different values for **4** and **6**: **4** is ca. 5 times more active after a continuative 72 h exposure, whereas the opposite result , i.e. a ca. 5-fold decrease of the cytotoxic activity, is found for compound **6** when cell treatment is prolonged from 24 to 72 h.

Most interestingly, compounds **1**, **4**, and **6** are all good PDT candidates because they are effective at mild light doses (10 J/cm^2) and show IC_{50} values 1 order of magnitude lower than those calculated in the dark in the same experimental conditions. Compounds **1** and **6** are the most potent and most promising because they already cause a significant reduction of tumor cells growth at a treatment dose as low as 1 J/cm^2.

Because the most common mechanism of action of the photosensitizers used in PDT (type II mechanism) involves the production of singlet oxygen upon photoexcitation, the $^1O_2$ quantum yield (Φ_Δ) was measured for compounds **1**, **4**, and **6**. Most PDT photosensitizers typically have singlet oxygen quantum yield values of ca. 0.5.[36] The investigated Ru−porphyrin conjugates have from moderate (Φ_Δ = 0.37 and 0.35 for **4** and **6**, respectively) to good (Φ_Δ = 0.63 for **1**) singlet oxygen quantum yields. These Φ_Δ values are not significantly different from those of the corresponding parent porphyrins (0.49, 0.38, and 0.40 for the precursors of **1**, **4**, and **6**, respectively). The phototoxicity of **1**, **4**, and **6** does not seem to be directly related to this parameter. In fact, **1** and **6** show the same potency in the phototoxic assay, despite **1** having a better singlet oxygen quantum yield compared to **6**. It is worth noting that Φ_Δ values are determined in ethanol solution and that most likely other parameters (e.g., hydrophobicity, cell uptake, ...) play a more significant role in determining the phototoxic activity of these conjugates under in vitro conditions.

The intracellular localization in MDA-MB-231 cells of compounds **1**, **4**, and **6** was determined after 16 h of exposure using fluorescence microscopy; the results for compound **6** are reported in Figure 7. The porphyrin-associated fluorescence revealed that **6** accumulates in not yet identified granular structures of the cytoplasm of the breast cancer cells (Figure 7B), yielding red emission spots, but not in the

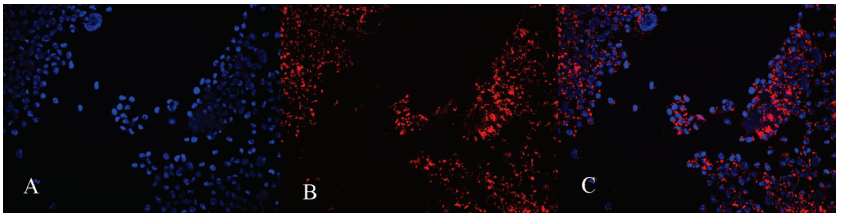

Figure 7. Evaluation of the intracellular localization of **6** in MDA-MB-231 human breast cancer cells by fluorescence microscopy. MDA-MB-231 cells were grown on histological glass slides and exposed to **6** (10 μM) for 16 h in the dark. Cells were fixed in 4% buffered formol, stained with DAPI, and examined (magnification 200×). (A) DAPI (excitation at 365 nm), (B) compound **6** (excitation at 535 nm), (C) overlay of excitation at 365 nm for DAPI staining of cell nuclei (blue) and excitation at 535 nm, indicating accumulation of **6** (red spots) in the cytoplasm of the cells.

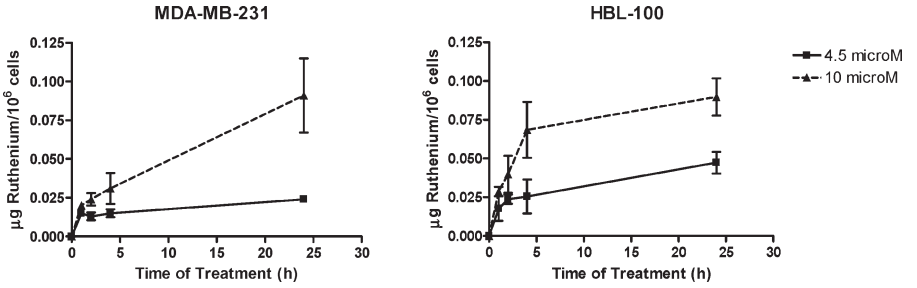

Figure 8. Ruthenium uptake in MDA-MB-231 and HBL-100 cells treated with compound **4**. Cells grown in multiwell plates were treated with compound **4** at 4.5 or 10 μM for 1, 2, 4, or 24 h. At the end of the treatment, ruthenium content was measured with atomic absorption spectroscopy.

nucleus, as demonstrated by the overlay with the blue fluorescence of DAPI (Figure 7C), a compound that selectively stains the nucleus (Figure 7A). Similar results were obtained with compounds **1** and **4** (data not shown). DAPI staining, several hours after treatment, did not show morphological changes at the nuclear level typical of apoptosis. On the basis of this observation, the most likely mechanism of cell death seems to be necrosis, consistent with literature data showing that both death mechanisms are possible in PDT, depending on the characteristics of the photosensitizing agent,[37] on the cell lines used[38], and on the treatment schedule used.[39]

The uptake of compound **4** by MDA-MB-231 and HBL-100 cells was measured by atomic absorption spectroscopy after treatment for 1, 2, 4, and 24 h. Compound **4** was selected because it is one of the conjugates with the highest positive charge (8+) and it shows different activity on the two cell lines (that might suggest different uptake). Two concentrations (4.5 and 10 μM) were used for each cell line that represent the IC_{50} values calculated for this compound in MDA-MB-231 and HBL-100 cells after a 72 h exposure, respectively. Figure 8 shows the μg of ruthenium/10^6 cells as a function of the time of treatment: in both cell lines, the ruthenium associated to cells increases proportionally to the duration of the treatment reaching approximately the same maximum value of 0.1 μg/10^6 cells in both cell lines (after 24 h at the concentration of 10 μM), although the accumulation kinetic seems slower in the human breast cancer cells in comparison to the nontumorigenic cells.

Thus, the large positive charge of the conjugate does not seem to inhibit its cellular uptake. Indeed, it has been demonstrated that highly charged metal complexes are capable of crossing cell membranes even better than neutral or low-positively charged species.[40]

Conclusions

We reported the preparation of two novel "extended-arms" versatile porphyrins, namely TetbpyPP and TedabpyPP, with a multistep approach and reasonable overall yield. These porphyrins, that bear at the *meso* positions four chelating bpy fragments connected through flexible linkers of different length and hydrophilicy, are particularly suited for the strong coordination of peripheral metal fragments. Thus, in principle, they might be easily exploited for the preparation of a wide array of conjugates in which the nature of the metal, the total charge, the presence of labile ligands, etc. can be varied on demand by an appropriate choice of the metal precursor. We demonstrated that both porphyrins can effectively bind four half-sandwich Ru(II) coordination compounds to give the tetra-cationic conjugates [TedabpyPP{Ru([9]aneS3)Cl}$_4$]Cl$_4$ (**6**) and [TetbpyPP{Ru([9]aneS3)Cl}$_4$]Cl$_4$ (**7**) in excellent yields. TedabpyPP seems to be best suited for biological purposes because the hydrophilic spacers, containing the ethylenedioxy groups, contribute to impart water solubility to the final compound: in fact, conjugate **6** is water-soluble, whereas **7** is totally insoluble. In contrast, conjugates of the highly hydrophobic 4′TPyP become water-soluble only when the charged metal fragments bear highly hydrophilic ligands, such as en, in their coordination sphere (e.g., compound **1**).

Compound **6**, together with the five other cationic Ru−porphyrin conjugates **1**−**5** recently described by us,[30] were investigated for in vitro cell growth inhibition toward MDA-MB-231 human breast cancer cells and HBL-100 human nontumorigenic epithelial cells. In the dark, all compounds showed IC_{50} values in the low micromolar range, i.e. at least 2 orders of magnitude lower than the corresponding Ru complexes. Their cytotoxic activity is scarcely dependent on the type of porphyrin and of Ru fragment. In other words, conjugation of the Ru(II) half-sandwich compounds to the porphyrin led to a remarkable increase of cytotoxicity, possibly due to improved uptake (see above). Interestingly, the two cell lines showed a different sensitivity to the cytotoxicity of compounds **4** and **6**, with the nontumorigenic HBL-100 much less affected than MDA-MB-231. Because the uptake is similar in the two cell lines, at least for **4**, this finding suggests the possibility of a specific interaction of **4** and **6** with a target differently expressed by the two cell lines.

Three compounds were selected for investigating their phototoxic effects on MDA-MB-231 human breast cancer cells upon illumination. Conjugates **1**, **4**, and **6** became ca. 10 times more cytotoxic after irradiation with visible light (590−700 nm) and proved to have from moderate to good singlet oxygen quantum yields. According to fluorescence microscopy experiments, they accumulate in the cytoplasm of the breast cancer cells but do not penetrate significantly into the nucleus. The most potent compounds **1** and **6** were active at nanomolar concentration and very low light dose (1 J/cm^2), making them promising sensitizers for the PDT of tumors.

Experimental Section

Mono and bidimensional (H−H COSY) ^{1}H NMR spectra were recorded at 400 or 500 MHz, respectively, on a JEOL Eclipse 400FT or on a Varian 500 spectrometer. All spectra were run at ambient temperature. In all the solvents chemical shifts were referenced to the peak of residual nondeuterated solvent (δ = 7.26 for $CDCl_3$, 5.32 for CD_2Cl_2, 3.31 for CD_3OD, 2.50 for DMSO-d_6). UV−vis spectra were obtained at T = 25 °C on a Jasco V-500 UV−vis spectrophotometer equipped with a Peltier temperature controller, using 1.0 cm path-length quartz cuvettes (3.0 mL). Electrospray mass spectra were recorded in the positive ion mode on a Bruker Esquire ESI-MS instrument. Fluorescence spectra were recorded on a F-4550 Hitachi spectrofluorimeter.

Column chromatography was performed on silica gel 60 Å (Merck, 230−400 mesh ASTM), eluting with dichloromethane/ethanol mixtures as specified below.

4-Methyl-2,2′-bipyridine-4′-carboxylic acid (bpyAc),[41] [4′TPyP-{Ru([9]aneS3)(en)}$_4$][CF_3SO_3]$_8$ (**1**), [4′TPyP{Ru([9]aneS3)(bpy)}$_4$]-[CF_3SO_3]$_8$ (**2**), [Bpy$_3$-PP{Ru([9]aneS3)(dmso-S)}$_3$][CF_3SO_3]$_6$ (**3**), [Bpy$_4$-PP{Ru([9]aneS3)(dmso-S)}$_4$][CF_3SO_3]$_8$ (**4**), and [Bpy$_4$-PP-{Ru([12]aneS4)}$_4$][NO_3]$_8$ (**5**) were prepared according to the published procedures.[30] All chemicals were purchased from Sigma-Aldrich and used without further purification unless otherwise specified.

The porphyrin−Ru conjugates precipitate with variable amounts of crystallization solvent that depend on the batch. For this reason, elemental analysis of such conjugates did not afford reliable and reproducible results and the values are not reported here (typically, some of the elemental analysis values, especially for C, differ from calculated values by > 0.5%). Nevertheless, the purity calculated from elemental analysis data was always > 95%, and the proposed formulas are all consistent with the ^{1}H NMR and ESI MS spectra.

Preparation of Compounds. 4-Formyl Benzoate. HCl (g) was bubbled for 30 min in a solution of 4-formylbenzoic acid (5 g, 0.33 mmol) dissolved in 250 mL of methanol and cooled in an ice bath. The mixture was heated to reflux for 30 min and evaporated to dryness under reduced pressure to obtain a white solid that was recrystallized from petroleum ether to obtain the title compound; yield 4.17 g (77%); mp = 60 °C (lit. 60 °C). ^{1}H NMR ($CDCl_3$, δ): 3.97 (s, 3H, CH_3), 7.96 (d, H3,5, J = 8.3 Hz), 8.20 (d, H2,6, J = 8.2 Hz), 10.11 (s, CHO).

***meso*-4′-Tetracarboxymethylphenylporphyrin (4′TCMePP).** A 2.30 g amount of methyl 4-formyl benzoate (14 mmol) in propionic acid (50 mL) was heated at 120 °C. Freshly distilled pyrrole (1.0 mL, 14 mmol) was added, and the mixture was refluxed for 1.5 h, then stored at −18 °C for 12 h. The purple precipitate was removed by filtration, thoroughly washed with cold methanol, and dried in vacuo at room temperature. Yield 0.63 g (21%). ^{1}H NMR ($CDCl_3$, δ): −2.81 (br s, 2H, NH), 4.12 (s, 12H, CH_3), 8.30 (d, 8H, *o*Ph, J = 8.1 Hz), 8.45 (d, 8H, *m*Ph, J = 8.1 Hz), 8.82 (s, 8H, Hβ). UV−vis (CH_2Cl_2, 25 °C) λ_{max}, nm (relative intensity, %): 420 (100), 515 (4.0), 550 (2.0), 590 (1.4), 646 (1.0).

***meso*-4′-Tetracarboxyphenylporphyrin (4′TCPP).** A 12 mL amount of a 40% KOH aqueous solution was added to a 200 mg amount of 4′TCMePP (0.236 mmol) dissolved in 200 mL of a 2:1 THF/CH_3OH mixture. The reaction mixture was stirred at 40 °C for 1 h, acidified with conc HCl (pH 5), and extracted with THF/CH_2Cl_2 1:1 (4 × 50 mL). The organic fraction was evaporated under reduced pressure, affording 174 mg of the desired purple product; yield: 93%. ^{1}H NMR (DMSO-d_6, δ): −2.94 (s, 2H, NH), 8.40 (m, 16H, *m*Ph + *o*Ph), 8.87 (s, 8H, βH), 13.32 (s, 4H, COOH). UV−vis (EtOH) λ_{max}, nm (relative intensity, %) 416 (100), 513 (4.2), 548 (2.1), 590 (1.3), 646 (0.9).

TedaNHBocPP. A 146 mg amount of EDCI (0.76 mmol) and a 103 mg amount of HOBt (0.76 mmol) were added to a solution of 4′TCPP (100 mg, 0.126 mmol) dissolved in 4 mL of anhydrous DMF. To this solution, after stirring for 30 min, a 138 mg amount of *N*-Boc-2,2′-(ethylenedioxy)diethylamine (0.56 mmol)[42] and a 68 mg amount of dimethylaminopyridine (DMAP) (0.56 mmol) dissolved in 1 mL of anhydrous DMF were added. The reaction mixture was shielded from light and stirred at room temperature for 24 h, and then the solvent was removed on a rotary evaporator to yield a dark semisolid. A 1:1 THF/CH_2Cl_2 mixture (100 mL) was added, and the organic layer was washed with water (40 mL × 3) and dried over anhydrous Na_2SO_4. The organic fraction was evaporated to dryness under vacuum, and the resulting solid was dissolved in 3 mL of CH_2Cl_2 and purified by column chromatography (4 × 20 cm) using CH_2Cl_2/EtOH (90:10) as eluent. The workup afforded 153 mg of the product as a purple solid (yield 72%). ^{1}H NMR ($CDCl_3$, δ): −2.83 (br s, 2H, NH), 1.38 (s, 36H, CH_3 Boc), 3.35 (m, 8H, CH_2 *spacer*), 3.61 (t, 8H, CH_2 *spacer*), 3.73 (m, 16H, CH_2 *spacer*), 3.84 (m, 16H, CH_2 *spacer*), 5.04 (br s, 4H, NHCO), 8.24 (dd, 16H, 8H *m*Ph + 8H *o*Ph), 8.81 (s, 8H, βH).

TetNHBocPP. A procedure similar to that described above was used, with the following parameters: 170 mg of 4′TCPP (0.215 mmol) in 10 mL of anhydrous DMF, 247.3 mg of EDCI (1.29 mmol), and 174 mg of HOBt (1.29 mmol). To this solution, a 275 mg amount of *N*-Boc-ethylenediamine[43] (1.72 mmol) was added and the reaction mixture stirred for 2.5 h at rt; yield 176 mg (60%). ^{1}H NMR ($CDCl_3$, δ): −2.84 (br s, 2H, NH), 1.48 (s, 36H, CH_3 Boc), 3.56 (m, 8H, CH_2NHCO), 3.74 (m, 8H, CH_2NHBoc), 5.09 (m, 4H, NHBoc), 7.57 (m, 8H, CH_2NHCO) 8.24 (dd, 16H, 8H mPh + 8H oPh, J = 8.22, 19.53 Hz), 8.79 (s, 8H, βH).

TedaNH$_2$PP·4CF$_3$SO$_3$H. A 6 mL amount of trifluoroacetic acid (TFA) was added to a solution of TedaNHBocPP (153 mg, 0.096 mmol) dissolved in 9 mL of anhydrous CH_2Cl_2. The mixture was shielded from light and stirred at room temperature for 2 h, after which the solvent was completely removed on a rotary evaporator to give a dark-green semisolid of the title porphyrin as triflate salt. A small amount (20 mg ca.) was neutralized with triethylamine (2 drops), dissolved in methanol (2 mL), precipitated with diethyl ether, filtered, and thoroughly washed with diethyl ether for characterization. ^{1}H NMR (free base) (CD_3OD, δ): 3.17 (t, 8H, CH_2NH_2), 3.80 (m, 40H, CH_2 *spacer*), 8.32 (dd, 16H, *m*Ph + *o*Ph), 8.90 (br s, 8H, βH). UV−vis (CH_3OH) λ_{max}, nm ($\varepsilon \times 10^{-3}$, dm^3 mol^{-1}cm^{-1}): 415 (479), 513 (20), 546 (11), 587 (7.1), 645 (5.9). ESI-MS m/z: 1312.7 (MH$^+$), 1334.6 (M + Na$^+$), 1350.6 (M + K$^+$).

The remaining product was used in the following step without further purification.

TetNH$_2$PP·4CF$_3$SO$_3$H. The same procedure as above was used, with the following parameters: 189 mg of TetNHBocPP (0.14 mmol) in 10 mL of anhydrous dichloromethane and 5 mL of TFA. ^{1}H NMR (free base) (DMSO-d_6, δ): −2.93 (s, 2H, NH), 3.13 (d, 8H, CH_2NH_2), 3.63 (d, 8H, $NHCH_2$), 8.35 (dd, 16H, *m*Ph + *o*Ph), 8.84 (m, 8H, βH), 9.11 (m, 4H, NHCO). ESI-MS (m/z): 959.4 (MH$^+$), 981.4 (M + Na$^+$) 791.2 (M(TCPP)H$^+$).

TedabpyPP. A 115 mg amount of bpyAc (0.54 mmol), a 155 mg amount of EDCI (0.81 mmol), and a 109 mg amount of HOBt (0.81 mmol) were dissolved in 5 mL of anhydrous DMF. After stirring for 30 min at room temperature, a solution of TedaNH$_2$PP (0.090 mmol) and 110 mg of DMAP (0.90 mmol) in 5 mL of anhydrous DMF was added. The reaction mixture was stirred for 24 h in the dark. At reaction completion

(TLC: aluminum oxide, CH_2Cl_2/EtOH 90:10), the solvent was evaporated under vacuum and the resulting solid was triturated with diethyl ether, filtered, thoroughly washed with diethyl ether, and dried in vacuum. Yield: 180 mg (96%). ^{1}H NMR (CD_2Cl_2, δ): −3.00 (s, 2H, NH), 2.21 (s, 12H, CH_3bpy), 3.68−3.83 (m, 48H, CH_2 *spacer*), 6.96 (d, 4H, J = 4.72 Hz, H5′), 7.21 (t, 4H, NHCO bpy), 7.31(t, 4H, NHCO), 7.66 (dd, 4H, J = 1.64, 4.96 Hz, H5), 8.10 (s, 4H, H3′), 8.10 (d, 8H, J = 7.95 Hz, *o*Ph), 8.18 (d, 8H, J = 7.95 Hz, *m*Ph), 8.35 (d, 4H, J = 4.96 Hz, H6′), 8.62 (d, 4H, J = 4.96 Hz, H6), 8.65 (s, 4H, H3), 8.74 (s, 8H, βH). ESI-MS m/z: 2096.7 (MH^+) 2118.6 ($M + Na^+$), 2134.5 ($M + K^+$). UV−vis (CH_3OH) λ_{max}, nm (relative intensity, %): 418 (100), 514 (4.7), 549 (2.4), 590 (1.5), 646 (1.1).

TetbpyPP. The same synthetic procedure as above was used, with the following parameters: 191 mg of bpyAc (0.89 mmol), 218 mg of EDCI (1.14 mmol), and 159 mg of HOBt (1.17 mmol) in 13 mL of anhydrous DMF. TetNH_2PP (0.14 mmol), 154 mg of DMAP (1.26 mmol) in 7 mL of anhydrous DMF. Yield: 181 mg (74%). ^{1}H NMR (DMSO-d_6, δ): −2.94 (br s, 2H, NH), 2.40 (s, 12H, CH_3), 3.64 (m, 16H, CH_2), 7.28 (d, 4H, H5′), 7.87 (d, 4H, H5), 8.26 (s, 4H, H3′), 8.31 (m, 16H, *o*Ph + *m*Ph), 8.57 (d, 4H, H6′), 8.84 (m, 16H, βH + H6 + H3), 9.00 (t, 4H, CONH), 9.16 (t, 4H, CONH). ESI-MS m/z: 1744.7 (MH^+), 1766.7 ($M + Na^+$), 1782.6 ($M + K^+$). UV−vis (CH_3OH + 5% DMSO) λ_{max}, nm ($\varepsilon \times 10^{-3}$, $dm^3\ mol^{-1}cm^{-1}$): 416 (237), 512 (13), 547 (7.1), 589 (5.1), 645 (3.8).

[TedabpyPP{Ru([9]aneS3)Cl}$_4$][Cl]$_4$ (6). A 50 mg amount of TedabpyPP (0.024 mmol) was dissolved in a mixture of CH_3OH (6 mL) and CH_2Cl_2 (2.5 mL). To this solution a 41 mg amount of [Ru([9]aneS3)(DMSO)Cl_2] (0.095 mmol) dissolved in 16 mL of hot CH_3OH was added. The mixture was refluxed for 24 h, and its color turned deep red. After reaction completion (TLC: aluminum oxide, CH_2Cl_2/EtOH 90:10), the solvent was evaporated under vacuum and the residue redissolved in a few drops of methanol. Dropwise addition of diethyl ether to the purple−brown solution induced the precipitation of a purple solid that was removed by filtration and washed repeatedly with diethyl ether and dried under vacuum at rt; yield 79 mg (92%). ^{1}H NMR (DMSO-d_6, δ): −2.93 (s, 2H, NH), 2.40−2.85 (m, 48H, CH_2 [9]aneS3), 2.53 (s, 12H, CH_3 bpy), 3.55 − 3.70 (m, 48H, CH_2 *spacer*) 7.50 (d, 4H, J = 5.03 Hz, H5′), 7.95 (d, 4H, J = 5.12 Hz, H5), 8.30 (s, 16H, *o*Ph + *m*Ph), 8.65 (s, 4H, H3′), 8.82 (d, 4H, J = 5.75 Hz, H6′), 8.84 (s, 8H, βH), 8.93 (t, 4H, CONH), 9.01 (s, 4H, H3), 9.11 (d, 4H, J = 5.74 Hz, H6), 9.27 (t, 4H, CONH). ESI-MS m/z: 841.5 (MH^+). UV−vis (CH_3OH) λ_{max}, nm (relative intensity, %): 417 (100), 513 (5.5), 549 (2.9), 590 (1.5), 645 (1.0).

[TetbpyPP{Ru([9]aneS3)Cl]$_4$}][Cl]$_4$ (7). The same synthetic procedure as above was used, with the following parameters: 25 mg of TetbpyPP (0.014 mmol) in 25 mL of CH_3OH and 27 mg of [Ru([9]aneS3)(DMSO)Cl_2] (0.063 mmol); yield, 39 mg (92%). ^{1}H NMR (DMSO-d_6, δ): −2.94 (br s, 2H, NH), 2.5−2.9 (m, 48H, CH_2 [9]aneS3), 7.49 (d, H5′), 8.03 (d, H5), 8.34 (dd, 16H, *o*Ph + mPh) 8.78 (s, H3′). 8.84 (m, 16H, βH + H6′), 9.17 (m, 12H, CONH + H3), 9.52 (m, 4H, CONH). UV−vis (CH_3OH) λ_{max}, nm (relative intensity, %): 417 (100), 513 (8.1), 548 (3.9), 589 (2.6), 645 (1.8).

Tumour Cell Lines for in Vitro Tests. The MDA-MB-231, highly invasive, human breast cancer cell line was kindly supplied by Dr. P. Spessotto (Cro, Aviano, Italy) and maintained in Dulbecco's modified Eagle's medium (EuroClone, Devon, UK) supplemented with 10% fetal bovine serum (FBS, Gibco, Invitrogen, Paisley, Scotland, UK), 2 mM L-glutamine (EuroClone, Devon, UK), 1% nonessential amino acids, and 100 IU/mL penicillin and 100 μg/mL streptomycin (EuroClone, Devon, UK).

The HBL-100 human nontumorigenic epithelial cell line was kindly supplied by Dr. G. Decorti (Department of Life Sciences, University of Trieste, Italy) and maintained in McCoy's 5A medium supplemented with 10% FBS, 2 mM L-glutamine, and 100 IU/mL penicillin and 100 μg/mL streptomycin.

Both cell lines were kept in a CO_2 incubator with 5% CO_2 and 100% relative humidity at 37 °C. Cells from a confluent monolayer were removed from flasks by a trypsin−EDTA solution. Cell viability was determined by the trypan blue dye exclusion test. For experimental purposes, cells were sown in multiwell culture clusters.

Determination of Cell Cytotoxicity. Cell growth inhibition was determined by the MTT viability test.[44] Cells sown on 96-well plates were incubated 24 h later with concentrations from 0.1 to 30 μM of the appropriate compound, prepared by dissolving it in a medium containing 5% of serum, for 72 h. Solutions of the conjugates **1**−**6** were prepared by diluting a freshly prepared stock solution (10^{-2} M) of each compound in DMSO (Sigma, St. Louis, MO). Maximum DMSO concentration in the cell incubation medium was ≤0.3% v/v. Cell toxicity analysis was performed at the end of the incubation time. Briefly, MTT dissolved in PBS (5 mg mL^{-1}) was added (10 μL per 100 μL of medium) to all wells and the plates were then incubated at 37 °C with 5% CO_2 and 100% relative humidity for 4 h. After this time, the medium was discarded and 200 μL of DMSO were added to each well according to the method of Alley et al.[45] Optical density was measured at 570 nm on a SpectraCount Packard (Meriden, CT) instrument. IC_{50} values were calculated from dose−effect curves with GraphPad Prism version 4.03 for Windows (GraphPad Software, San Diego, CA).

Determination of Cell Phototoxicity. Cells grown in 96-well cell culture plates were incubated 24 h later with concentrations from 0.1 to 10 μM of compounds **1**, **4**, and **6**, prepared by dissolving them in a medium containing 5% of serum, for 24 h. Stock DMSO solutions of each conjugate were prepared as described above. Maximum DMSO concentration in the cell incubation medium was ≤0.1% v/v. Thereafter, the media containing compounds were replaced with drug-free medium containing 5% of serum and cells were irradiated at 590−700 nm at a fluence rate of 25 mW/cm^2 and light doses ranging from 1 to 10 J/cm^2. This wavelength interval was isolated from the emission of a halogen lamp (Teclas, Lugano, Switzerland) by the insertion of broadband optical filters. Control experiments performed in the absence of any photosensitizer indicated that light doses up to 10 J/cm^2 cause no evident cell damage. A plate similarly treated but not exposed to light was used as reference for the dark cytotoxicity in the same experimental conditions. Experiments were conducted in quadruplicate and repeated trice. Analysis of cell phototoxicity using the MTT assay as described above was performed after a further incubation of 24 h after irradiation and compared to the values of control cells without light irradiation.

Determination of the Quantum Yield for Singlet Oxygen Generation. The quantum yield (Φ_Δ) of singlet oxygen generated by compounds **1**, **4**, and **6** upon photoexcitation was measured using 9,10-dimethylanthracene (DMA) as substrate.[46] Typically, 1.5 mL of a 20 μM ethanol solution of DMA and 1.5 mL solution of the porphyrin (0.4 A at Soret band maximum, ≈ 10^{-6} M) in ethanol were placed in a quartz cuvette of 1 cm optical path and irradiated with 590−700 nm light for different periods of time at 20 ± 2 °C under gentle magnetic stirring. The fluence rate was 100 mW/cm^2. The DMA fluorescence emission was recorded in the 380−550 nm wavelength range with excitation at 360 nm. The first-order rate constant of the photo-oxidation of DMA by $^1O_2$ was obtained by plotting ln F_0/F as a function of the irradiation time t, where F_0 and F represent the fluorescence intensity at time 0 and at time t, respectively. The rate constant was then converted into $^1O_2$ quantum yield by comparison with the rate constant for DMA photo-oxidation sensitized by hematoporphyrin (Hp), for which Φ_Δ was shown to be 0.65.[47]

Microscopy Experiments. MDA-MB-231 cells were grown on histological slides in complete medium until 75% confluence was reached and exposed to compounds **1**, **4**, and **6** (10 μM) for

16 h in the dark. At the end of the treatment, after discarding the medium containing the compound and washing, cells were fixed for 10 min in buffered formol, and nuclei were stained with 4′,6-diamino-2-phenylindolyl hydrochloride (DAPI, Molecular Probes, Invitrogen, Italy) according to the manufacturer's instructions. Then slides were mounted with 20% PBS-glycerol and analyzed under a fluorescence microscope (Leica, DM 2000, Italy) with filters set at 365 ± 5 nm excitation light (BP 340/380, FT 400, LP 425) for DAPI, and 535 ± 25 nm excitation light (BP 515−560, FT 580, LP 590) for porphyrins.

Determination of Ruthenium Cell Uptake. Ruthenium cell uptake was determined by atomic absorption spectroscopy (AAS) on samples processed with a modification of the procedure by Tamura and Arai.[48] MDA-MB-231 and HBL-100 cells were seeded in complete medium containing 5% of serum in a 6-well plate. When cells reached 75% confluence, they were incubated with 4.5 or 10 μM of compound **4** for 1, 2, 4, or 24 h at 37 °C. At the end of the treatment, the wells were washed three times with PBS, the cells collected by a trypsin/EDTA solution, counted with the trypan blue exclusion test, and the intracellular concentration of ruthenium was determined. The cells were dried in Nalgene cryogenic vials (a first drying step was performed overnight at 80 °C and a second step at 105 °C until the samples reached a constant weight). The dried cells were decomposed by the addition of an aliquot of tetramethylammonium hydroxide (25% in water) (Aldrich) and of Milli-Q water at a ratio of 1:1 directly in each vial at room temperature under shaking. Final volumes were adjusted to 1 mL with Milli-Q water. The concentration of ruthenium in treated cells was measured by flameless atomic absorption spectroscopy using a Zeeman graphite tube atomizer, model SpectrAA-300, equipped with a specific ruthenium emission lamp (hollow cathode lamp P/N 56-101447-00, Varian, Mulgrave, Victoria, Australia). Quantification of ruthenium was carried out in 10 μL samples at 349.9 nm with an atomizing temperature of 2500 °C, using argon as carrier gas at a flow rate of 3.0 L/min. Before each analysis, a five-point calibration curve was obtained to check the range of linearity using ruthenium custom-grade standard 998 mg/mL (InorganicVentures, Lakewood, NJ).

Statistical Analysis. Data obtained in the experiments were subjected to Statistical Analysis of Variance (ANOVA) and Tukey-Kramer post-test, or to Unpaired *t* test performed using GraphPad InStat version 3.06 for Windows (GraphPad Software, San Diego, CA, USA).

Acknowledgment. Sincere acknowledgements are due to: Regione FVG (Project "Nuove Terapie e Farmaci Antitumorali"), Fondo Trieste, and Fondazione Beneficentia Stiftung for financial support; BASF Italia Srl for a generous donation of hydrated ruthenium chloride; Dr. Paolo Durigutto for the helpful assistance in the acquisition of fluorescence microscopy images. Fondazione CRTrieste is also gratefully acknowledged for the munificent donation of a Varian 500 NMR spectrometer to the Department of Chemical Sciences. This study was performed within the frame of COST Action D39.

Supporting Information Available: Mono and bidimensional NMR spectra (TetbpyPP, TedabpyPP, **7**), UV−vis spectra (time course for **6**), comparative fluorescence spectra for TedabpyPP and **6**, cell viability of control cells exposed or not to different total light doses, photobleaching of DMA by compound **1**. This material is available free of charge via the Internet at http://pubs.acs.org.

References

(1) (a) Levina, A.; Mitra, A.; Lay, P. A. Recent developments in ruthenium anticancer drugs. *Metallomics* **2009**, *1*, 458–470. (b) Bruijnincx, P. C.; Sadler, P. J. Controlling platinum, ruthenium, and osmium reactivity for anticancer drug design. In *Adv. Inorg. Chem*., van Eldik, R., Hubbard, C. D., Eds.; Elsevier: Amsterdam, 2009, pp 1−62. (c) Bruijnincx, P. C.; Sadler, P. J. New trend for metal complexes with anticancer activity. *Curr. Opin. Chem. Biol*. **2008**, *12*, 197–206. (d) Ang, W. H.; Dyson, P. J. Classical and nonclassical ruthenium-based anticancer drugs: towards targeted chemotherapy. *Eur. J. Inorg. Chem*. **2006**, *20*, 4003–4018. (e) Clarke, M. J. Ruthenium metallopharmaceuticals. *Coord. Chem. Rev*. **2003**, *236*, 209–233. (f) Clarke, M. J.; Zhu, F.; Frasca, D. R. Non-platinum chemotherapeutic metallopharmaceuticals. *Chem. Rev*. **1999**, *99*, 2511–2534.

(2) (a) Bratsos, I.; Jedner, S.; Gianferrara, T.; Alessio, E. Ruthenium anticancer compounds: challenges and expectations. *Chimia* **2007**, *61*, 692–697. (b) Alessio, E.; Mestroni, G.; Bergamo, A.; Sava, G. Ruthenium antimetastatic agents. *Curr. Top. Med. Chem*. **2004**, *4*, 1525–1535. (c) Alessio, E.; Mestroni, G.; Bergamo, A.; Sava, G. Ruthenium anticancer drugs. *Met. Ions Biol. Syst*. **2004**, *42*, 323–351.

(3) (a) Jakupec, M. A.; Galanski, M.; Arion, V. B.; Hartinger, C. G.; Keppler, B. K. Antitumour metal compounds: more than theme and variations. *Dalton Trans*. **2008**, 183–194. (b) Hartinger, C. G.; Zorbas-Seifried, S.; Jakupec, M. A.; Kynast, B.; Zorbas, H.; Keppler, B. K. From bench to bedside—preclinical and early clinical development of the anticancer agent indazolium trans-[tetrachlorobis(1H-indazole)ruthenate(III)] (KP1019 or FFC14A). *J. Inorg. Biochem*. **2006**, *100*, 891–904.

(4) Rademaker-Lakhai, J. M.; van den Bongard, D.; Pluim, D.; Beijnen, J. H.; Schellens, J. H. M. A Phase I and pharmacological study with imidazolium-*trans*-DMSO-imidazole-tetrachlororuthenate, a novel ruthenium anticancer agent. *Clin. Cancer Res*. **2004**, *10*, 3717–3727.

(5) Hartinger, C. G.; Jakupec, M. A.; Zorbas-Seifried, S.; Groessl, M.; Egger, A.; Berger, W.; Zorbas, H.; Dyson, P. J.; Keppler, B. K. KP1019, a new redox-active anticancer agent: preclinical development and results of a clinical phase I study in tumor patients. *Chem. Biodiversity* **2008**, *5*, 2140–2155.

(6) Bergamo, A.; Sava, G. Ruthenium complexes can target determinants of tumour malignancy. *Dalton Trans*. **2007**, 1267–1272.

(7) (a) Peacock, A. F. A.; Sadler, P. J. Medicinal organometallic chemistry: designing metal arene complexes as anticancer agents. *Chem. Asian J*. **2008**, *3*, 1890–1899. (b) Dougan, S. J.; Sadler, P. J. The design of organometallic ruthenium arene anticancer agents. *Chimia* **2007**, *61*, 704–715. (c) Yan, Y. K.; Melchart, M.; Habtemariam, A.; Sadler, P. J. Organometallic chemistry, biology and medicine: ruthenium arene anticancer complexes. *Chem. Commun*. **2005**, 4764–4776. (d) Chen, H.; Parkinson, J. A.; Morris, R. E.; Sadler, P. J. Highly selective binding of organometallic ruthenium ethylenediamine complexes to nucleic acids: novel recognition mechanisms. *J. Am. Chem. Soc*. **2003**, *125*, 173–186.

(8) (a) Bergamo, A.; Masi, A.; Dyson, P. J.; Sava, G. Modulation of the metastatic progression of breast cancer with an organometallic ruthenium compound. *Int. J. Oncol*. **2008**, *33*, 1281–1289. (b) Vock, C. A.; Renfrew, A. K.; Scopelliti, R.; Juillerat-Jeanneret, L.; Dyson, P. J. Influence of the diketonato ligand on the cytotoxicities of $[Ru(\eta^6\text{-}p\text{-cymene})\text{-}(R_2acac)(PTA)]^+$ complexes (PTA = 1,3,5-triaza-7-phosphaadamantane). *Eur. J. Inorg. Chem*. **2008**, 1661–1671. (c) Dyson, P. J. Systematic design of a targeted organometallic antitumor drug in preclinical development. *Chimia* **2007**, *61*, 698–703.

(9) (a) Grguric-Sipka, S.; Stepanenko, I. N.; Lazic, J. M.; Bartel, C.; Jakupec, M. A.; Arion, V. B.; Keppler, B. K. Synthesis, X-ray diffraction structure, spectroscopic properties and antiproliferative activity of a novel ruthenium complex with constitutional similarity to cisplatin. *Dalton Trans*. **2009**, 3334–3339. (b) Nováková, O.; Nazarov, A. A.; Hartinger, C. G.; Keppler, B. K.; Brabec, V. DNA interactions of dinuclear Ru^{II} arene antitumor complexes in cell-free media. *Biochem. Pharmacol*. **2009**, *77*, 364–374. (c) Mendoza-Ferri, M. G.; Hartinger, C. G.; Nazarov, A. A.; Kandioller, W.; Severin, K.; Keppler, B. K. Modifying the structure of dinuclear ruthenium complexes with antitumor activity. *Appl. Organomet. Chem*. **2008**, *22*, 326–332. (d) Mendoza-Ferri, M. G.; Hartinger, C. G.; Eichinger, R. E.; Stolyarova, N.; Jakupec, M. A.; Nazarov, A. A.; Severin, K.; Keppler, B. K. Influence of the spacer length on the in vitro anticancer activity of dinuclear ruthenium-arene compounds. *Organometallics* **2008**, *27*, 2405–2407.

(10) (a) Das, S.; Sinha, S.; Britto, R.; Somasundaram, K.; Samuelson, A. G. Cytotoxicity of half sandwich ruthenium(II) complexes with strong hydrogen bond acceptor ligands and their mechanism of action. *J. Inorg. Biochem*. **2010**, *104*, 93–104. (b) Meggers, E.; Atilla-Gokcumen, G. E.; Gründler, K.; Frias, C.; Prokop, A. Inert ruthenium half-sandwich complexes with anticancer activity. *Dalton Trans*. **2009**, 10882–10888. (c) Camm, K. D.; El-Sokkary, A.; Gott, A. L.; Stockley, P. G.; Belyaeva, T.; McGowan, P. C. Synthesis, molecular structure and evaluation of new organometallic ruthenium anticancer agents.

Dalton Trans. **2009**, 10914–10925. (d) Ruiz, J.; Vicente, C.; de Haro, C.; Bautista, D. A novel ruthenium(II) arene based intercalator with potent anticancer activity. *Dalton Trans*. **2009**, 5071–5073.

(11) For a very recent review article about Ru-arene compounds with anticancer properties see: Süss-Fink, G. Arene ruthenium complexes as anticancer agents. *Dalton Trans*. **2010**, *39*, 1673–1688.

(12) Serli, B.; Zangrando, E.; Gianferrara, T.; Scolaro, C.; Dyson, P. J.; Bergamo, A.; Alessio, E. Is the aromatic fragment of piano-stool ruthenium compounds an essential feature for anticancer activity? The development of new Ru(II)-[9]aneS3 analogues. *Eur*. *J*. *Inorg*. *Chem*. **2005**, 3423–3434.

(13) Bratsos, I.; Jedner, S.; Bergamo, A.; Sava, G.; Gianferrara, T.; Zangrando, E.; Alessio, E. Half-sandwich Ru^{II}-[9]aneS3 complexes structurally similar to antitumor-active organometallic piano-stool compounds: preparation, structural characterization and in vitro cytotoxic activity. *J*. *Inorg*. *Biochem*. **2008**, *102*, 1120–1133.

(14) (a) Lottner, C.; Bart, K.-C.; Bernhardt, G.; Brunner, H. Hematoporphyrin-derived soluble porphyrin−platinum conjugates with combined cytotoxic and phototoxic antitumor activity. *J*. *Med*. *Chem*. **2002**, *45*, 2064–2078. (b) Lottner, C.; Bart, K.-C.; Bernhardt, G.; Brunner, H. Soluble tetraarylporphyrin-platinum conjugates as cytotoxic and phototoxic antitumor agents. *J*. *Med*. *Chem*. **2002**, *45*, 2079–2089.

(15) Mao, J. F.; Zhang, Y. M.; Zhu, J. H.; Zhang, C. L.; Guo, Z. J. Molecular combo of photodynamic therapeutic agent silicon(IV) phthalocyanine and anticancer drug cisplatin. *Chem*. *Commun*. **2009**, 908–910.

(16) (a) Ben-Hur, E.; Chan, W.-S. Phthalocyanines in photobiology and their medical applications. In *The Porphyrin Handbook*; Kadish, K. M., Smith, K. M., Guilard, R., Eds.; Academic Press: Boston, 2003; Vol. 19, pp 1−35. (b) Pandey, R. K.; Zheng, G. Porphyrins as photosensitizers in photodynamic therapy. In *The Porphyrin Handbook*; Kadish, K. M., Smith, K. M., Guilard, R., Eds.; Academic Press: Boston, 2000; Vol. 6, pp 157−230.

(17) Nyman, E. S.; Hynninen, P. H. Research advances in the use of tetrapyrrolic photosensitizers for photodynamic therapy. *J*. *Photochem*. *Photobiol*., *B* **2004**, *73*, 1–28.

(18) Detty, M. R.; Gibson, S. L.; Wagner, S. J. Current clinical and preclinical photosensitizers for use in photodynamic therapy. *J*. *Med*. *Chem*. **2004**, *47*, 3897–3915.

(19) MacDonald, I. J.; Dougherty, T. J. Basic principles of photodynamic therapy. *J*. *Porphyrins Phthalocyanines* **2001**, *5*, 105–129.

(20) DeRosa, M. C.; Crutchley, R. J. Photosensitized singlet oxygen and its applications. *Coord*. *Chem*. *Rev*. **2002**, *233*−*234*, 351–371.

(21) Weersink, R. A.; Bogaards, A.; Gertner, M.; Davidson, S. R. H.; Zhang, K.; Netchev, G.; Trachtenberg, J.; Wilson, B. C. Techniques for delivery and monitoring of TOOKAD (WST09)-mediated photodynamic therapy of the prostate: clinical experience and practicalities. *J*. *Photochem*. *Photobiol*., *B* **2005**, *79*, 211–222.

(22) (a) Farrer, N. J.; Salassa, L.; Sadler, P. J. Photoactivated chemotherapy (PACT): the potential of excited-state d-block metals in medicine. *Dalton Trans*. **2009**, 10690–10701. (b) Szaciłowski, K.; Macyk, W.; Drzewiecka-Matuszek, A.; Brindell, M.; Stochel, G. Bioinorganic photochemistry: frontiers and mechanisms. *Chem*. *Rev*. **2005**, *105*, 2647–2694. (c) Ali, H.; van Lier, J. E. Metal complexes as photo- and radiosensitizers. *Chem*. *Rev*. **1999**, *99*, 2379–2450.

(23) (a) Song, R.; Kim, Y.-S.; Lee, C. O.; Sohn, Y. S. Synthesis and antitumor activity of DNA binding cationic porphyrin−platinum-(II) complexes. *Tetrahedron Lett*. **2003**, *44*, 1537–1540. (b) James, B. R.; Meng, G. G.; Posakony, J. J.; Ravensbergen, J. A.; Ware, C. J.; Skov, K. A. Porphyrins and metalloporphyrins: potential hypoxic agents. *Met*.*-Based Drugs* **1996**, *3*, 85–89. (c) Ding, L.; Etemad-Moghadam, G.; Cros, S.; Auclair, C.; Meunier, B. Syntheses and in vitro evaluation of water-soluble "cationic metalloporphyrin−ellipticine" molecules having a high affinity for DNA. *J*. *Med*. *Chem*. **1991**, *34*, 900–906.

(24) (a) Sun, R. W.-Y.; Che, C.-M. The anti-cancer properties of gold(III) compounds with dianionic porphyrin and tetradentate ligands. *Coord*. *Chem*. *Rev*. **2009**, *253*, 1682–1691. (b) To, Y. F.; Sun, R. W.-Y.; Chen, Y.; Chan, V. S.-F.; Yu, W.-Y.; Tam, P. K.-H.; Che, C.-M.; Lin, C.-L. S. Gold(III) porphyrin complex is more potent than cisplatin in inhibiting growth of nasopharyngeal carcinoma in vitro and in vivo. *Int*. *J*. *Cancer*. **2009**, *124*, 1971–1979. (c) Wang, Y.; He, Q.-Y.; Sun, R. W.-Y.; Che, C.-M.; Chiu, J.-F. Cellular pharmacological properties of gold(III) porphyrin 1a, a potential anticancer drug lead. *Eur*. *J*. *Pharmacol*. **2007**, *554*, 113–122. (d) Wang, Y.; He, Q.-H.; Sun, R. W.-Y.; Che, C.-M.; Chiu, J.-F. Gold(III) porphyrin 1a induced apoptosis by mitochondrial death pathways related to reactive oxygen species. *Cancer Res*. **2005**, *65*, 11553–11564.

(25) (a) Vicente, M. G. H. Porphyrin-based sensitizers in the detection and treatment of cancer: recent progress. *Curr*. *Med*. *Chem*. *Anticancer Agents* **2001**, *1*, 175–194. (b) Tronconi, W.; Colombo, A.; Decesare, M.; Marchesini, R.; Woodburn, K. W.; Reiss, J. A.; Phillips, D. R.; Zunino, F. Biodistribution of haematoporphyrin analogues in a lung carcinoma model. *Cancer Lett*. **1995**, *88*, 41–48. (c) Woodburn, K. W.; Phillips, D. R.; Bellinger, G. C. A.; Sadek, M.; Brownlee, R. T. C.; Reiss, J. A. Synthesis and phototoxicity of a series of haematoporphyrin analogues. *Bioorg*. *Med*. *Chem*. *Lett*. **1992**, *2*, 343–344.

(26) (a) Gullotti, E.; Yeo, Y. Extracellularly activated nanocarriers: a new paradigm of tumor targeted drug delivery. *Mol*. *Pharmaceutics* **2009**, *6*, 1041–1051. (b) Maeda, H. The enhanced permeability and retention (EPR) effect in tumor vasculature: the key role of tumor-selective macromolecular drug targeting. *Adv*. *Enzyme Regul*. **2001**, *41*, 189–207. (c) Baban, D. F.; Seymour, L. W. Control of tumour vascular permeability. *Adv*. *Drug Delivery Rev*. **1998**, *34*, 109–119.

(27) Gabrielsson, A.; Lindsay Smith, J. R.; Perutz, R. N. Remote site photosubstitution in metalloporphyrin−rhenium tricarbonylbipyridine assemblies: photoreactions of molecules with very short lived excited states. *Dalton Trans*. **2008**, 4259–4269.

(28) (a) Schmitt, F.; Govindaswamy, P.; Zava, O.; Süss-Fink, G.; Juillerat-Jeanneret, L.; Therrien, B. Combined arene ruthenium porphyrins as chemotherapeutics and photosensitizers for cancer therapy. *J*. *Biol*. *Inorg*. *Chem*. **2009**, *14*, 101–109. (b) Schmitt, F.; Govindaswamy, P.; Süss-Fink, G.; Han Ang, W.; Dyson, P. J.; Juillerat-Jeanneret, L.; Therrien, B. Ruthenium porphyrin compounds for photodynamic therapy of cancer. *J*. *Med*. *Chem*. **2008**, *51*, 1811–1816.

(29) (a) Rani-Beeram, S.; Meyer, K.; McCrate, A.; Hong, Y.; Nielsen, M.; Swavey, S. A fluorinated ruthenium porphyrin as a potential photodynamic therapy agent: synthesis, characterization, DNA binding, and melanoma cell studies. *Inorg*. *Chem*. **2008**, *47*, 11278–11283. (b) Davia, K.; King, D.; Hong, Y.; Swavey, S. A porphyrin−ruthenium photosensitizer as a potential photodynamic therapy agent. *Inorg*. *Chem*. *Commun*. **2008**, *11*, 584–586.

(30) Gianferrara, T.; Bratsos, I.; Iengo, E.; Milani, B.; Oštrić, A.; Spagnul, C.; Zangrando, E.; Alessio, E. Synthetic strategies towards ruthenium−porphyrin conjugates for anticancer activity. *Dalton Trans*. **2009**, 10742–10756.

(31) Gianferrara, T.; Giust, D.; Bratsos, I.; Alessio, E. Metalloporphyrins as chemical shift reagents: the unambiguous NMR characterization of the *cis*- and *trans*-isomers of *meso*-(bis)-4′-pyridyl-(bis)-4′-carboxymethylphenylporphyrins. *Tetrahedron* **2007**, *63*, 5006–5013.

(32) Gianferrara, T.; Serli, B.; Zangrando, E.; Iengo, E.; Alessio, E. Pyridylporphyrins peripherally coordinated to ruthenium-nitrosyls, including the water-soluble $Na_4[Zn\cdot 4'TPyP\{RuCl_4(NO)\}_4]$: synthesis and structural characterization. *New J*. *Chem*. **2005**, *29*, 895–903.

(33) (a) Lauceri, R.; Purrello, R.; Shetty, S. J.; Vicente, M. G. H. Interactions of anionic carboranylated porphyrins with DNA. *J*. *Am*. *Chem*. *Soc*. **2001**, *123*, 5835–5836. (b) Ribo, J. M.; Crusats, J.; Farrera, J.-A.; Valero, M. L. Aggregation in water solutions of tetrasodium diprotonated meso-tetrakis(4-sulfonatophenyl)porphyrin. *J*. *Chem*. *Soc*., *Chem*. *Commun*. **1994**, 681–682.

(34) (a) Barrett, A. J.; Kennedy, J. C.; Jones, R. A.; Nadeau, P.; Pottier, R. H. The effect of tissue and cellular pH on the selective biodistribution of porphyrin-type photochemotherapeutic agents: a volumetric titration study. *J*. *Photochem*. *Photobiol*., *B* **1990**, *6*, 309–323. (b) Cohen, L.; Schwartz, S. Modification of radiosensitivity by porphyrins: II. Transplanted rhabdomyosarcoma in mice. *Cancer Res*. **1966**, *26*, 1769–1773.

(35) Gianferrara, T.; Bratsos, I.; Alessio, E. A categorization of metal anticancer compounds based on their mode of action. *Dalton Trans*. **2009**, 7588–7598.

(36) Ochsner, M. Photophysical and photobiological processes in the photodynamic therapy of tumours. *J*. *Photochem*. *Photobiol*., *B* **1997**, *39*, 1–18.

(37) He, X. Y.; Sikes, R. A.; Thomsen, S.; Chung, L. W.; Jacques, S. L. Photodynamic therapy with photofrin II induces programmed cell death in carcinoma cell lines. *Photochem*. *Photobiol*. **1994**, *59*, 468–473.

(38) Dahle, J.; Steen, H. B.; Moan, J. The mode of cell death induced by photodynamic treatment depends on cell density. *Photochem*. *Photobiol*. **1999**, *70*, 363–367.

(39) (a) Luo, Y.; Chang, C. K. Initiation of apoptosis versus necrosis by photodynamic therapy. *Photochem*. *Photobiol*. **1996**, *66*, 479–483. (b) Bugelsky, P. J.; Porter, C. W.; Dougherty, T. J. Autoradiographic distribution of hematoporphyrin derivate in normal and tumour tissue of the mouse. *Cancer Res*. **1981**, *41*, 4606–4612.

(40) (a) Klein, A. V.; Hambley, T. W. Platinum drug distribution in cancer cells and tumors. *Chem*. *Rev*. **2009**, *109*, 4911–4920. (b) Kapp, T.; Dullin, A.; Gust, R. Mono- and polynuclear [alkylamine]platinum(II) complexes of [1,2-bis(4-fluorophenyl)ethylenediamine]platinum(II): synthesis and investigations on cytotoxicity, cellular distribution, and DNA and protein binding. *J*. *Med*. *Chem*. **2006**, *49*,

1182–1190. (c) Harris, A. L.; Yang, X.; Hegmans, A.; Povirk, L.; Ryan, J. J.; Kelland, L.; Farrell, N. P. Synthesis, characterization, and cytotoxicity of a novel highly charged trinuclear platinum compound. Enhancement of cellular uptake with charge. *Inorg. Chem.* **2005**, *44*, 9598–9600.

(41) McCafferty, D. G.; Bishop, B. M.; Wall, C. G.; Hughes, S. G.; Mecklenberg, S. L.; Meyer, T. J.; Erickson, B. W. Synthesis of redox derivatives of lysine and their use in solid-phase synthesis of a light-harvesting peptide. *Tetrahedron* **1995**, *51*, 1093–1106.

(42) Beer, P. D.; Cadman, J.; Lloris, J. M.; Martínez-Máñez, R.; Soto, J.; Pardo, T.; Marcos, M. D. Anion interaction with ferrocene-functionalised cyclic and open-chain polyaza and aza-oxa cycloalkanes. *J. Chem. Soc., Dalton Trans.* **2000**, 1805–1812.

(43) Kofoed, T.; Hansen, H. F.; Orum, H.; Koch, T. Synthesis and fluorescent labeling of beta-amyloid peptides. *J. Peptide Sci.* **2001**, *7*, 402–412.

(44) Mosman, T. Rapid colorimetric assay for cellular growth and survival: application to proliferation and cytotoxicity assays. *J. Immunol. Methods* **1983**, *65*, 55–63.

(45) Alley, M. C.; Scudiero, D. A.; Monks, A.; Hursey, M. L.; Czerwinski, M. J.; Fine, D. L.; Abbott, B. J.; Mayo, J. G.; Schoemaker, R. H.; Boyd, M. R. Feasibility of drug screening with panels of human tumor cell lines using a microculture tetrazolium assay. *Cancer Res.* **1988**, *48*, 589–601.

(46) Gross, E.; Ehrenberg, B.; Johnson, F. Singlet oxygen generation by porphyrins and the kinetics of 9,10-dimethyl-anthracene photosensitization in liposomes. *Photochem. Photobiol.* **1993**, *57*, 808–813.

(47) Fabris, C.; Vicente, M. G. H.; Hao, E.; Friso, E.; Borsetto, L.; Jori, G.; Miotto, G.; Colautti, P.; Moro, D.; Esposito, J.; Ferretti, A.; Rossi, C. R.; Nitti, D.; Sotti, G.; Soncin, M. Tumour-localizing and -photosensitising properties of *meso*-tetra(4-nido-carboranylphenyl)porphyrin (H_2TCP). *J. Photochem. Photobiol., B* **2007**, *89*, 131–138.

(48) Tamura, H.; Arai, T. Determination of ruthenium in biological tissue by graphite furnace AAS after decomposition of the sample by tetramethylammonium hydroxide. *Bunseki Kagaku* **1992**, *41*, 13–17.